Quasi-Static Crushing and Energy Absorption Characteristics of Thin-Walled Cylinders with Geometric Discontinuities of Various Aspect Ratios

Abstract

In this paper, energy absorption and deformation capacity of circular thin-walled members with elliptical cut-outs are investigated both numerically and experimentally. Thin-walled members possess the uniform height, thickness, average cross sectional area, material and volume are subjected to axial quasi-static loading. To conduct such tests, special fixture arrangement is designed for placing the specimen in the compression loading machine. The deformation mechanisms and the corresponding collapse mode along with its energy absorption of the thin-walled tubes were investigated in detail for various aspect ratios (0.315, 0.523, 0.854, 1, 3.375 and 4.08). The explicit finite element code ABAQUS was then employed to perform the numerical studies inview of mitigating the influence of cutout shape, location and symmetry on energy absorption and crush characteristics. In aspect ratio of 4.08, whose major axis length of 24.5 mm observed maximum crash force efficiency (CFE) of 14% possessing symmetric discontinuity. The results of experimental and simulations are in good agreement and shows that the location and symmetry of cutouts had considerable effect on collapse crushing behaviour.

N. Baaskaran [a]
K. Ponappa [a]
S. Shankar [b]

[a] Department of Mechanical Engineering, Kongu Engineering college, Erode, Tamil Nadu-638052, India.
Email: baaskararcher@kongu.ac.in, ponappa@kongu.ac.in

[c] Department of Mechatronics Engineering, Kongu Engineering college, Erode, Tamil Nadu-638052, India.
Email: shankar@kongu.ac.in

http://dx.doi.org/10.1590/1679-78253866

1 INTRODUCTION

In the recent years, high speed logistics maximizes the probability of fatal accidents which leads to high rate of injuries during vehicular crashes. The tubular structures exhibits significant energy absorption capability when subjected to impact loading, results in minimizing the injuries during collision. The availability of various materials and cross sections can be chosen for the energy absorbing elements in vehicles. However, unlike the aluminum which is chosen in the absence of con-

ventional steel structures which results in the 25% of overall weight reductions. The positioning of aluminum columns behind the bumpers paves the way to protect the structure and occupants during collision. It is possible, by absorbing the initial kinetic energy and significantly less reduction in force levels which can be tolerable by commuters that develops during collision. The 50 kN of force level can be tolerated by humans without the maximum damage during collision (Jones., 2011). The structure geometry, material properties, discontinuities and the loading conditions are the dominant factors in formation of deformation modes of high speed steel (HSS) extrusions. They also reported that the effect of strain rate and strain hardening effects of collapse behavior of thin-walled tubes are limited. Additionally, the geometric discontinuities such as cutouts and stiffeners in real time scenarios leads to stress concentration adjacent to the cut-outs that affects the crushing pattern of the structure (Reid et al., 1986). The axi-symmetrical fold pattern was observed in quasi-static loading during experimental scheme when cylindrical shells are subjected to various loading conditions (Dorin et al., 2017). The theoretical static plastic hinge model was developed to derive the basic expression for mean crushing force (Abramowicz et al., 1984). Energy absorbers are one the passive safety systems employed in automotive industry, also known as crash boxes. The main purpose of using energy absorbers is to control the impact energy of the automobile during crash. The aluminum is becoming more familiar in replacing the conventional steel materials due to the high strength to weight ratio and excellent formability. In case of absorbing impact, the superior energy absorbing properties can be rendered by aluminum combined with intelligent crash box design leads to bigger shape and lesser weight when compare to conventional steel energy absorber. During the recent years, the attention focused on light weight structures and crashworthiness to envisage the analytical, experimental and finite element approaches to interpret the peak force, mean force, collapse mode and energy absorbed (Szwedowicz et al., 2014); (Wierzbicki et al., 1983); (Hou et al., 2007); (Tai et al., 2010); (Zahran et al., 2017).

The introduction of crush initiators without discontinuities results in cutting and splitting deformation pattern, it was observed instead of global deformation in thin-walled members. The behavior of steel and aluminum tubes in the influence of square cut-outs when subjected to dynamic impact and quasi-static loading. The formation of major axis in positioning the geometrical irregularities at mid-zone is reported. At most priority is to improvise the energy absorption pattern of 12.54% and reduction in peak load values by 10.52% by introducing circular and elliptic discontinuities with-out much rise in overall structural weight (Estrada et al., 2016). The local responses are generated near the cut-out, when the shell structure is subjected to impact load. The axial crushing of thin-walled members results in non-uniform load-displacement pattern which is not desired. The amplitude of the first peak collapse load, which is correlated with the plastic hinges, is greater than the rest of other obtained peaks (Nia et al., 2012); (Chukwuemeke et al., 2016); (Hou et al., 2007). The energy absorbing capability of the structure mainly depends upon the formation of first plastic fold occurred during deformation (Estrada et al., 2016). Normally in automotive sector, weight factor is also one of the major area as well as energy absorption, the aim of the designer is to achieve maximum energy absorption with lesser weight. There are also some applications where only less weight energy absorbers can employed. They are sacrificial cladding structure in which the energy absorbers are arranged in particular orientation in the civil structures in view of protecting

the main load members from the air blast loads (Explosions) (Palanivelu et al., 2011); (Velmurugan et al., 2009).

Many studies have been conducted to study the quasi-static progressive crushing of thin-walled tubes; it reveals the origin of deformation pattern occurred at the concentrated end of structure experiencing impulse loading. Moreover, the deformation occurs either asymmetrically (Mode-Diamond) nor asymmetrically (Mode-Ring (or) Concertina) which is determined by (D/t) ratio. The experimental results show that the thin-walled tubes possessing higher D/t (>80) is very susceptible to strain-hardening leads to diamond mode deformation and tubes with D/t (<80) is completely rigid-plastic (low strain hardening), the occurrence of deformation is in concertina mode. The correlation between the diameter to wall thickness ratio (D/t) and length to wall thickness ratio (L/t), its impact on prediction of deformation pattern is given (Alexander et al., 1960); (Hsu et al., 2004); (Chung et al., 2008). This work has been further refined on switching over the occurrence of deformation pattern from diamond to concertina and concertina to mixed collapse modes. The energy absorption capacity is vitally influenced by mean collapse load. (Khalkhali et al., 2016) This exhibits the development of theoretical models in determining the mean collapse loads for square and circular cross-sections experiencing axisymmetric and asymmetric collapse modes. The strain rate effect plays a crucial role in improvement of yield stress of material. (Huang et al., 2014)They suggested an improved method in determining the expression for dynamic loading using quasi-static mean crush load.

To the author's knowledge, abundant information is needed at the instant, regarding the folding pattern of aluminum structures with cut-outs. The explicit finite element code ABAQUS was employed to perform an economic and efficient analysis for evaluating the quasi-static collapse mode and energy absorption characteristics inclusion of cut-outs in thin-walled structures. In order to assess the collapse characteristics, with various elliptical shape discontinuities pattern was performed numerically and experimentally by quasi-static axial crushing tests. The obtained results are compared with the numerical data and more information about crush progressive responses are generated. The comparative studies are undergone to demonstrate the impact of elliptical shaped discontinuities to undermine the optimal positioning of cut-outs in thin–walled tubes.

2 TEST SPECIMEN AND EXPERIMENTAL SET-UP

2.1 Specimens

In our work, the specimens are made using Aluminum 2024 alloy, which is shown in Figure 1.

2.2 Material Property

Aluminum alloys are mainly chosen as energy absorbers due to their light weights. In this research work, Aluminum 2024 (Inox metal works, Mumbai) of Diameter (D) =52 mm, length (L) =120 mm and thickness (t) =0.0102 mm is opted. The D/t ratio is then 5098, it indicates the structure can be treated as thin walled tubes. Young's modulus E=69000 Mpa and poisson's ratio v=0.35 and the corresponding material properties are given in Table 1.

Figure 1: Specimen mounted on the fixtures using the lathe machine.

Johnson-Cook Material parameters						Cowper-Symonds parameters				
Material	Density (Kg/m^3)	A (Mpa)	B (Mpa)	C_P (J/Kg K)	T_{melt} (K)	n	c	m	C(s^{-1})	p
Al 2024	277	265	426	875	775	0.34	0.015	1.0	6500	4

T_{melt}= melting temperature; C_P=Sp. Heat capacity; A, B, n, c, m, C and P are material constants.

Table 1: The material parameters.

2.3 Mounting of the Specimen

The specimen was firmly fixed on the mounting fixture as depicted in Figure 1. The lathe machine was employed to mount the specimen and cross section of the entire setup is shown in Figure 2 and 3. The headstock is employed to accommodate the inner part of the top mounting fixture, although the inner part of bottom mounting fixture was almost in taper which can be supported by tailstock. Hence, the end faces of both bottom and top of clamping fixtures should be in parallel before pre-ceding the mounting of specimen. Then the specimen is carefully mounted on to the inner part of the top mounting fixture and spindle axis should be aligned accordingly. The bottom mounting fixture was inserted to the rear end of the specimen and rigidly fastened by 12 (M6) screws on both the ends. The transition fit is employed between the outer diameter of the inner parts of mounting flange and inner diameter of the specimen to ensure that the specimen should be pushed to the inner sector of mounting fixtures by small force. The specimen can be pushed gradually; the occurrence of deformation in the axial direction due to the contact radial thrust of the specimen by fastening of screw is negligible. Furthermore, the elastic deformation could be occurred due to the misalignment of the center-axis of the specimen. It can be retain to its original shape and occurrence of shift (curved) to its neutral axis, when the mounting fixture released from lathe centers. The procedure is done at utmost care to minimize the stresses acting on the specimen and check the end faces of bottom and top of clamping fixtures were parallel.

Figure 2: Exhibits the installed
specimen on mounting fixture.
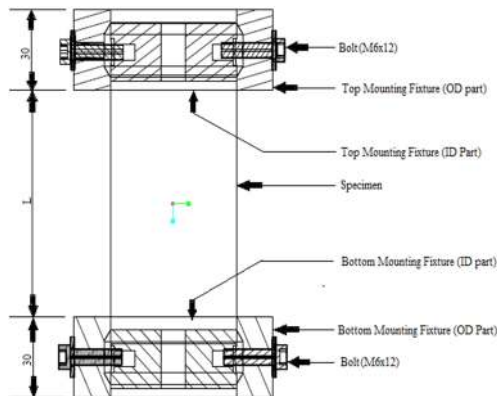
Figure 3: Exhibits the schematic cross section of
the specimen installed on mounting fixture.

2.4 Experimental Setup

The axial quasi-static loading of specimen is carried out using DEEPAK (DTRX) hydraulic machine as shown in Figure 4. This machine has two jaws: the upper one is movable and the lower one is stationary, it is equipped with 30 kN load cell which was used for quasi-static axial compression tests.

The specimen is placed between the two jaws in vertical direction which enables the specimen to get compressed axially. Since the upper and the lower jaws of the machine are movable and stationary, consequently, the upper and lower ends of the specimen are noted as "Fixed end" and Moving end" correspondingly. To attain accuracy, three samples of each specimen were tested and the obtained mean value was treated as the final result. The quasi-static compression is accomplished by compressing the specimen at the controlled displacement rate of 5 mm/min until the thin-walled tubes experiencing the limited crush. The other researchers have applied the cross head speed between the range of 5 and 10 mm/min to ensure the absence of dynamic effects while testing (Niknejad et al., 2012); (Ahmad et al., 2009); (Kashani et al., 2013); (Estrada et al., 2016). In Table 2, the values of the maximum and mean forces captured in these tests are listed along with crushing length of the sample at the end of process, starting location of the collapse process, type of collapse modes and these terms associated with energy absorption which is calculated from load-displacement pattern. The in-built automatic data acquisition system was utilized to capture the above parameters in the testing. Results of the quasi-static compression process of thin walled cut-out tubes are utilized for validation of numerical simulation in the upcoming sections.

Specimen No	P_{max} (N)	P_{mean} (N)	$E_{absorbed}$ (J)	Deformation (mm)	Collapse mode	Collapse Starting point	CFE (%)	SEA (J/Kg)
Pr14	434	54.78	5.03	96	Diamond	Mid of Specimen	12.62	2129.97
Pr24	509	49.01	5.64	92.3	Diamond	Mid of Specimen	9.62	2403.15
Pr34	376	56.31	4.75	96.67	Diamond	Mid of Specimen	14.97	2024.27
Pr44	532	32.92	2.59	89.3	Diamond	Moving End	6.18	1258.18
Pr54	488	54.83	4.50	94	Diamond	Mid of Specimen	11.23	1913.37
Pr64	572	50.65	5.14	91.67	Diamond	Mid of Specimen	8.85	2195.81

Table 2: Average values of the important results for cut-outs length $L_0 = 0.75$ mm (Experimental results).

3 NUMERICAL SIMULATIONS

3.1 Description of Numerical Model

The general geometry and FEM model of the thin-walled tubes considered in this study is shown in Figure 5. The parameters involved for all modeled configurations were similar as experimental and the various Lo were examined. The Lo can be termed as the distance between the centers of cut-outs to the bottom end of the tube. The material behavior including the post-yield response was defined using the Johnson–cook parameters which are depicted in Table.1. The fixed and movable jaws of the testing machine base were modeled using two rigid surfaces located on the fixed and moving end of the specimen. The three-dimensional shell element S4R are much opted to model the quasi-static process; the advancing front algorithm is used to generate the mesh refinement on the edges of the cut-out. The local seeds of approximate element size of 2.5 mm for a total of 2243 quadrilateral dominated element were used for free meshing. The R3D4 rigid elements were employed to model the fixed and moving ends.

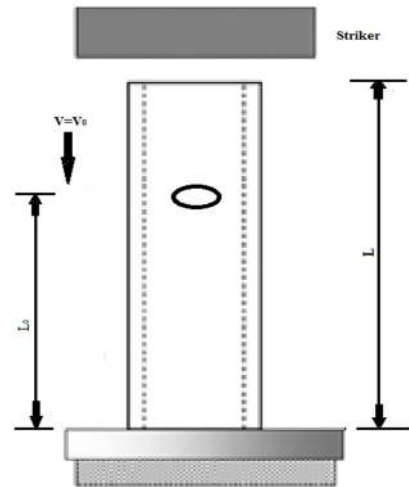
Figure 4: Deepak DTRX apparatus.

Figure 5: Schematic view of FEM and geometric model.

The interactions between the specimen and the movable jaw can be created using general contact algorithm with the friction co-efficient of 0.2. The upper end of the tube is subjected to velocity via the movable top rigid surface. In actual (Experimental) quasi-static process, the loading rate was applied as 5 mm/min, if the same loading rate is chosen for simulation it is too slow which in turn increases the time step significantly. In view of reducing the time step of the process, the artificial ramping of velocity of 0.3 m/s is applied on movable top rigid surface. Furthermore, the loading rate is smooth as possible to prevent the abrupt movements which can propagate the noisy signals, stress waves which may paves way to obtain in-accurate solutions. The initial slope and velocity is equal to initial acceleration which is to be zero that can be observed from typical smooth loading curve. It assures the gradual loading through-out the process by avoiding the dynamic effects involved. Similarly, the quasi-static analysis was performed by employing AMPLITUDE and SMOOTHSTEP suboption for controlling the applied velocity was reported (Khalkhali et al., 2016); (Fan et al., 2013).

3.2 Expression for Surface Area of Thin-Walled Tubes Including Elliptical Cut-Out (Huang et al., 2010)

Considering a thin-walled tube which was intersected with a hollow circular pipe whose cross-section is of ellipse with radii p and q. The thin-walled tube along with an elliptic cut-out is shown in Figure 6, the elliptic cut-out geometry can be expressed by the equation (1)
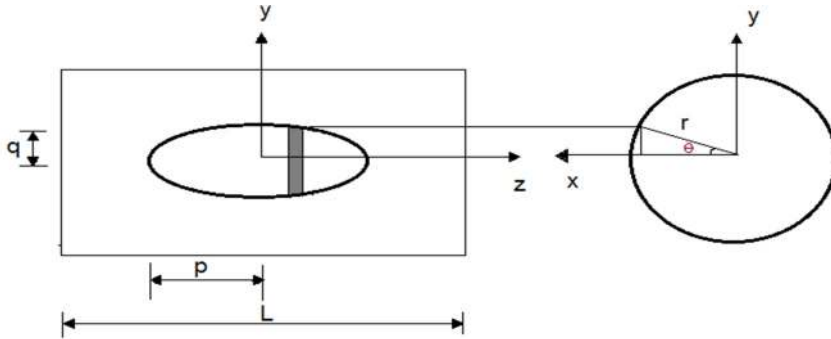
$$y = q\left(\sqrt{1 - \frac{z^2}{p^2}}\right) \tag{1}$$

Figure 6: Geometry of thin-walled tube with elliptic-cutout.

For analytical study, the small strip which is generated by slicing of the tube as exposed as dark zone in the Figure 6. It should satisfy the cut-out boundary, area of this strip can be written as,

$$dA = 2r\theta.dz \tag{2}$$

The relation between θ and y is configured from Figure 6

$$Sin\ \theta = \frac{y}{r} \tag{3}$$

The θ can be obtained by substituting the Equation (1) in (3),

$$\theta = sin^{-1}\left(\frac{q}{r}\right)\left(\sqrt{1 - \frac{z^2}{p^2}}\right) \tag{4}$$

By substituting Equation (4) in (2), we get

$$dA = 2r\ sin^{-1}\left(\frac{q}{r}\right)\left(\sqrt{1 - \frac{z^2}{p^2}}\right).dz \tag{5}$$

The overall cut-out surface area A^*, can be calculated by integrating the equation (5), in the following form:

$$A^* = \int_{-a}^{a} 2r\, sin^{-1}\left(\frac{q}{r}\right)\left(\sqrt{1 - \frac{z^2}{p^2}}\right).dz \tag{6}$$

It can be refined as

$$A^* = 4r \int_{0}^{a} 2r\, sin^{-1}\left(\frac{q}{r}\right)\left(\sqrt{1 - \frac{z^2}{p^2}}\right).dz \tag{7}$$

This form is considered as constraint equation, which can be rewritten as $A^* = \frac{A}{\alpha}$ or

$$4r \int_{0}^{a} 2r\, sin^{-1}\left(\frac{q}{r}\right)\left(\sqrt{1 - \frac{z^2}{p^2}}\right).dz = A = \frac{2\pi r L}{\alpha} \tag{8}$$

4 RESULTS AND DISCUSSION

The results of experimental and numerical data are compared in Table 3. From the above tables, the maximum variation of results observed is about10.34 %. Herewith, numerical simulations can foresee the characteristics of thin-walled tubes behavior fairly. Moreover, the other parameters like energy absorption, mean and maximum forces observed are more or less same for both in numerical and experiments. Even though there is also some variation in the formation and starting point of collapse modes can be which can be depicted in Table 3.

Specimen No	Difference%				Collapse mode	Collapse Starting Point
	P_{max} (N)	P_{mean} (N)	$E_{absorbed}$ (J)	Deformation (mm)		
Pr14	8.41	4.66	10.34	-6.61	Similar	Different
Pr24	5.06	1.72	4.53	-5.64	Similar	Different
Pr34	2.69	7.24	-10.32	-5.52	Similar	Similar
Pr44	6.49	-6.35	6.58	-4.53	Similar	Similar
Pr54	-2.92	4.28	-8.54	-2.31	Similar	Different
Pr64	4.54	-3.74	7.12	-1.36	Similar	Different

Table 3: Comparison between the results of simulations and experiments cut-outs length L_0 =0.75 mm.

The logic behind the variation may be due to the preparation of specimen by forming and welding process. The change in collapse mode is mainly due to the formation of starting locations of fold, it can be happen by flawed approximation of friction co-efficient in numerical modeling. Till now, there is lack of in availability of deterministic criterion for predicting the starting point of collapse modes (Nia et al., 2010). It provokes the results obtained in experiments are more authentic. There are varieties of parameters involved in characterizing the crashworthiness of thin-walled structures. The first parameter is the total energy absorbed which can be calculated by the work done by the crushing force in longitu-dinal deformation (Δ) can be expressed in following equation (9). The second important parameter is the mean load (P_{mean}), which can be calculated using equation (10). It is the measure of average forces required to compress the material in form of progressive folding.

The third parameter is the specific energy absorption (SEA), which provides the ability of energy absorption capability per unit mass of the crushed structural component and expressed in equation (11). The crush force efficiency (CFE) is the fourth parameter shown in equation (12), provokes the idea about the energy absorption behavior about the ideal structural component. Here the ideal value is considered as 100%, which indicates initiation of crushing (P_{max}) load is constant and remains the same. The lower CFE is not preferred because of higher initial force is directly transferred to the mounting structure.

$$E_a = \int_0^\Delta F.d\Delta \tag{9}$$

$$P_{mean} = \frac{\int_0^{lmax} F(l).dl}{l_{max}} \qquad (N) \tag{10}$$

$$SEA = \frac{\int_0^{lmax} F(l).dl}{M_{bc}} \qquad (J/Kg) \tag{11}$$

$$CFE = \frac{p_{mean}}{p_{max}} \qquad (\%) \tag{12}$$

4.1 The Impact of Location of the Cutout

The cut-out size of 1/45 of the overall area of the tube was created at different locations along the length of tubes. The elliptical cut-outs were positioned at five different locations of L_0 (L_0=0.375, 0.5, 0.625, 0.75 and 0.875), the variation in three different major axis lengths and aspect ratios were chosen as geometric discontinuities to mitigate the effect of location in this section. The explicit relationship between radii p and q for the shell with an elliptical cut-out is shown in Figure 7.
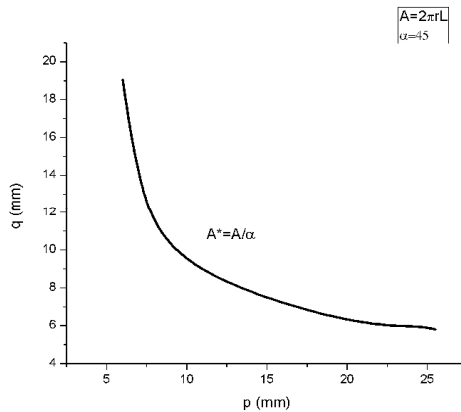

Figure 7: Relation between radii of p and q of an elliptic cutout on thin-walled tubes.

The major axis of the cut-outs refers to the longitudinal axis of discontinuities which is perpendicular to the direction of quasi-static loading. Figure 8 shows the fabricated specimens which is to be subjected to quasi-static loading, the comparison between collapse modes of samples (Pr14 and 24) in experiments and simulations are depicted in Figure 9.
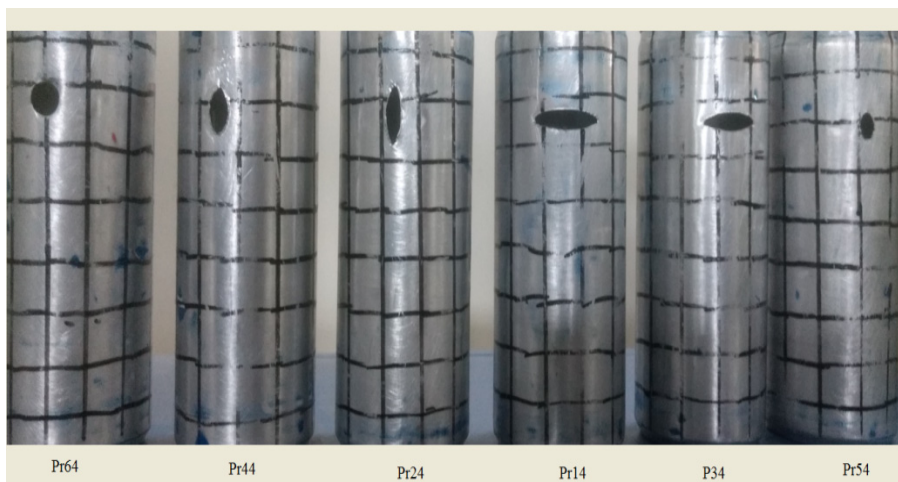
Figure 8: Fabricated specimen subjected to quasi-static loading.
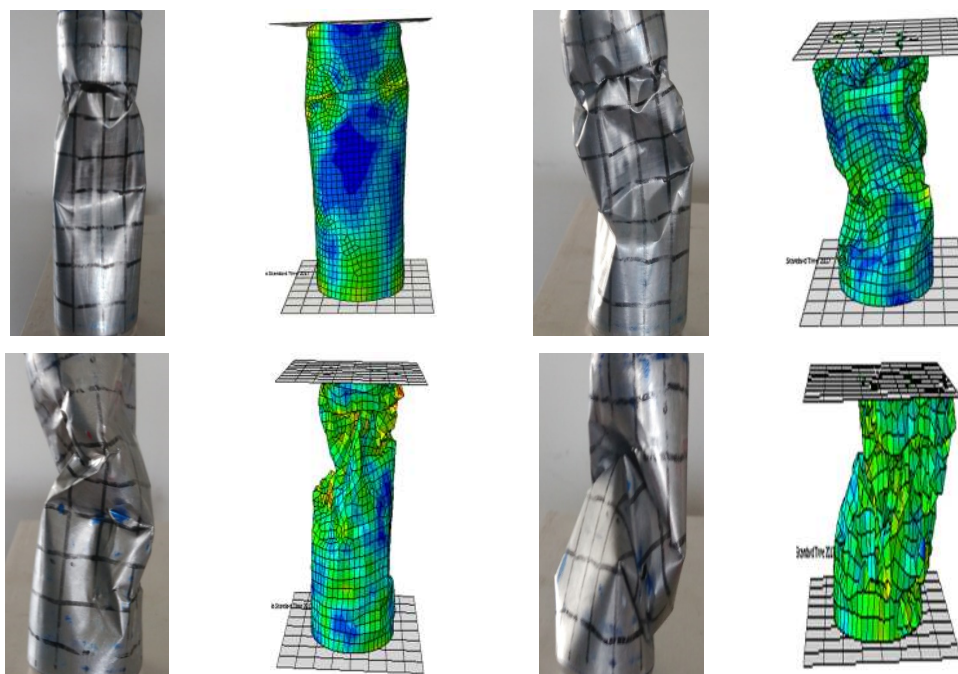
Figure 9: Comparison between collapse modes of samples in experiments and simulations (Pr14 and Pr24).

The analogous force-deformation and energy absorption deformation pattern of thin-walled tubes with a cutout subjected to quasi-static loading are depicted in Figure 10 and Table 4, 5 appropriately. Additionally, the specimen without cutout also included in the above study for benchmarking. When the cutout locations are positioned at 0.5 and 0.625L, the occurred deformation is greater due to global bending and as the position of cutout advanced nearer to the loading end (0.875 and 0.75L) results in halt in deformation before it reaches the crushing length of 110 mm.

Specimen No	Geometric Description					Analytic Results			
	Shape	$L_0(L)$	Minor axis (mm)	Major axis (mm)	Aspect Ratio (mm)	P_{max} (N)	P_{mean} (N)	$E_{absorbed}$ (J)	Deformation (mm)
Pr00			NO	NO	NO	568.49	56.512	4.684	105.074
Pr11		0.375	24.5	6	4.08	413.31	39.014	3.226	104.639
Pr12		0.5				384.98	36.28	3.056	104.052
Pr13		0.625				395.67	43.961	3.975	102.582
Pr14		0.75				389.25	52.574	4.608	102.346
Pr15		0.875				405.11	54.877	4.877	101.327
Pr16		0.75				169.81	23.779	5.504	102.417
Pr21		0.375	6	19.04	0.315	483.60	49.096	3.621	100.102
Pr22		0.5				505.47	50.367	3.712	98.807
Pr23		0.625				477.41	51.112	2.981	97.281
Pr24		0.75				485.89	52.668	5.359	97.514
Pr25		0.875				513.57	53.287	4.097	96.563
Pr26		0.75				417.57	45.565	4.715	97.689
Pr31		0.375	20.25	6	3.375	435.24	35.311	2.833	103.987
Pr32		0.5				416.87	44.278	3.331	103.442
Pr33		0.625				397.20	45.481	3.930	101.538
Pr34		0.75				414.81	52.229	4.625	101.723
Pr35		0.875				442.06	57.386	5.077	99.416
Pr41		0.375	7	13.37	0.523	519.62	42.897	2.341	96.474
Pr42		0.5				516.63	48.854	4.267	95.321
Pr43		0.625				502.65	50.821	4.025	95.468
Pr44		0.75				496.97	35.010	2.766	93.758
Pr45		0.875				546.61	59.105	5.118	93.287
Pr51		0.375	7	8.2	0.854	530.63	48.949	4.073	99.471
Pr52		0.5				545.51	47.865	4.034	97.939
Pr53		0.625				545.92	42.537	3.365	96.522
Pr54		0.75				529.68	52.481	4.638	96.179
Pr55		0.875				556.20	57.744	4.907	96.143
Pr61		0.375	9	9	1.0	502.97	40.254	3.241	96.581
Pr62		0.5				536.84	43.335	3.427	95.673
Pr63		0.625				493.18	46.342	3.854	95.292
Pr64		0.75				531.26	52.550	4.913	92.943
Pr65		0.875				547.77	53.646	4.502	93.547
Pr66		0.75				460.29	51.478	5.413	93.783

Table 4: Numerical simulation of circular thin-walled tubes with one or two cut-outs placed at various locations.

The above result clearly reveals that two locations (i.e., 0.875 and 0.75L) lead to local buckling around the location of the cut-out. The occurred local buckling around the cut-out location results in absence of global bending and similar occurrence was observed in previous literature (Huang et al., 2010). To provoke the complete information regarding the change in deformation, this can be obtained by considering the end-shortening of thin-walled tubes up to 110 mm numerically. The outcome observed clearly reveals the location of the cut-out along the shell's length vertically; possess greater impact on energy absorbing capability. As we noticed from Table 4 & 5, there were only the slight variations in the first peak forces as the location of cut-outs varied from 0.75 to 0.875 L. It is followed by sudden reduction of crushing force which is invariable to the cutout location due

to the formation of plastic hinges. But the observed pattern of entire collapse mode is different; this behavior is already cited in various literatures. The collapse mode is much similar for the tubes whose location of cut-outs positioned in 0.75 to 0.875 L, had the maximum proximity to the loading end, results in similar energy absorbing capability.

Specimen No	Geometric Description					Analytic Results			
	Shape	L_0 (L)	Minor axis (mm)	Major axis (mm)	Aspect Ratio (mm)	Collapse mode	Collapse Starting point	CFE (%)	SEA (J/Kg)
Pr00			NO	NO	NO	C and D	ME	9.940	1983.06
Pr11		0.375	24.5	6	4.08	D	MOS	9.439	1365.79
Pr12		0.5				D	MOS	9.423	1293.81
Pr13		0.625				C and D	MOS	11.110	1606.68
Pr14		0.75				C and D	ME	13.506	1950.88
Pr15		0.875				D	ME	13.546	2064.77
Pr16		0.75				D	ME	14.003	2330.22
Pr21		0.375	6	19.04	0.315	D	MOS	9.155	1541.50
Pr22		0.5				D	MOS	8.977	1580.24
Pr23		0.625				D	MOS	7.797	1269.05
Pr24		0.75				D	ME	9.901	2281.39
Pr25		0.875				D	ME	9.559	1744.14
Pr26		0.75				D	ME	10.911	2007.23
Pr31		0.375	20.25	6	3.375	D	MOS	8.112	1206.55
Pr32		0.5				D	MOS	10.621	1418.65
Pr33		0.625				D	MOS	11.450	1673.76
Pr34		0.75				C and D	ME	12.590	1969.76
Pr35		0.875				D	ME	12.981	2162.26
Pr41		0.375	7	13.37	0.523	D	MOS	6.020	995.32
Pr42		0.5				D	MOS	9.862	1814.97
Pr43		0.625				D	MOS	9.816	1712.03
Pr44		0.75				D	ME	7.044	1176.52
Pr45		0.875				D	ME	10.812	2176.94
Pr51		0.375	7	8.2	0.854	C and D	MOS	9.224	1729.51
Pr52		0.5				D	MOS	9.017	1712.95
Pr53		0.625				D	MOS	7.791	1428.87
Pr54		0.75				C and D	ME	9.907	1969.42
Pr55		0.875				C and D	ME	10.381	2083.65
Pr61		0.375	9	9	1.0	D	MOS	8.003	1382.67
Pr62		0.5				D	MOS	8.072	1462.03
Pr63		0.625				C and D	MOS	9.396	1644.19
Pr64		0.75				D	ME	9.891	2095.99
Pr65		0.875				C and D	ME	9.793	1920.64
Pr66		0.75				D	ME	11.183	2309.30

[a] Collapse Mode - C and D (Concertina and Diamond), D (Diamond)

[b] Collapse Starting Point – ME (Moving End), MOS (Mid of Specimen), FE (Fixed end)

Table 5: Numerical simulation of circular thin-walled tubes with one or two cut-outs placed at various locations.

The above location clarifies the propagation of local buckling without causing global bending on the peripheral surface of the cutout. The occurred buckling is stable throughout the process resulting in progressive irregular folding, due to the uniform accumulated force around the cutout loca-

tion. Furthermore, if the cutout is positioned at the mid-portion of tube results in change of transformation from progressive buckling to global bending mode is the major cause for energy absorbing capability. The energy absorbing capabilities were depicted in Figure 11, the P_{mean} for Pr11, Pr21, Pr31 and Pr41 are 39.01, 49.09, 35.31 and 42.89 N respectively. It clearly reveals the reduction of energy absorption by 30.9, 13.13, 37.51 and 24.10% when compared to the absence of cutout in the tube. The occurrence of stable deformation observed in position of cutout location in 0.75 L and elliptical discontinuity of aspect ratio of 1.
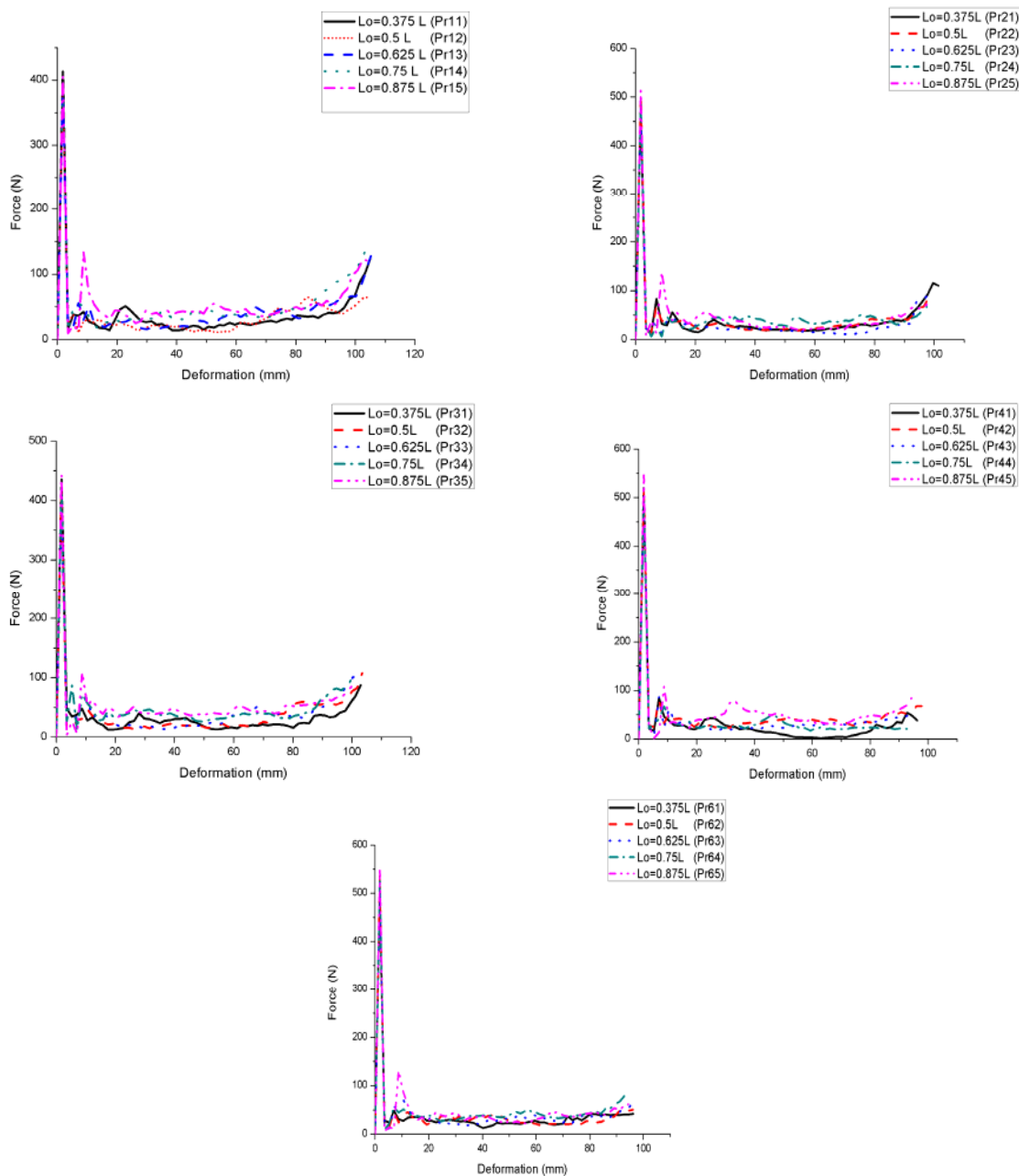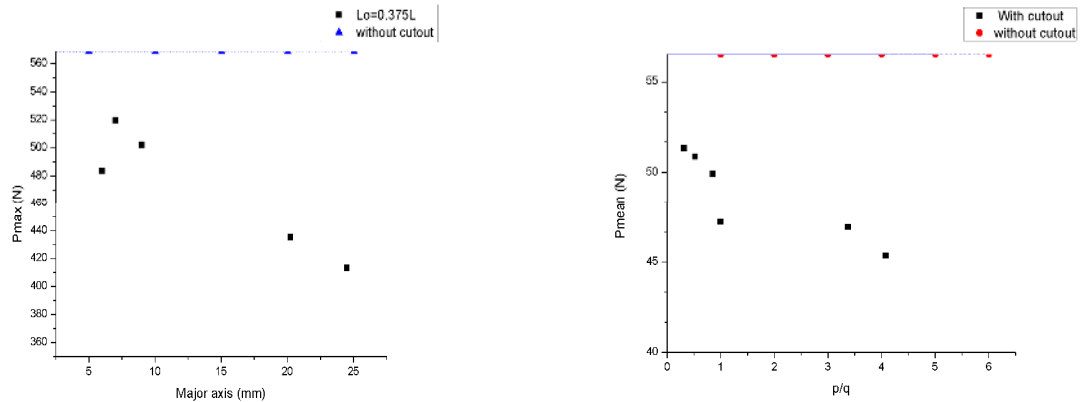

Figure 10: a) Force Vs Deformation.

Figure 11: a) Max.Peak Force Vs Major axis at (Lo=0.375L)   b) Mean forcé Vs Aspect ratio (p/q).

Consequently, the P_{mean} was observed to reduce significantly with the increase in aspect ratios and the load carrying capability is greatly influenced by cutouts indirectly by aspect ratios. The resistance offered by the tube is much greater when the major axis is minimum and narrow, perpendicular to the quasi-static compression loading. The pattern is completely in contrast of long major and short minor axis, the resistance offered is comparatively low when the cutout is narrow. The position directly influences the occurrence of collapse mode and its corresponding load bearing capacity.

4.2 The Impact of Aspect Ratio of the Cutout

The energy absorption capability of thin-walled tubes under the influence of different aspect ratios and geometric discontinuities are investigated in this section. It is evident that the collapse behavior is mainly affected by position of cutout location at 0.75L rather than 0.875L. Additionally, to verify the results obtained, Figure 11 a) depicts the behavior of thin walled tubes variation in major axis to the maximum peak force. It is clear that change in major axis had direct influence on occurrence of peak load and corresponding deformation. For instance, the major axis length positioned at Lo=0.375L shows reduction in major axis results in decrease in maximum peak force of 27.36%, 14.96%, 23.41%, 8.62% and 11.61% for the five types of cutout (Pr11, Pr21, Pr31, Pr41 and Pr41) respectively. The occurred deformation of cutouts of major axis 24.5 mm and 9 mm are about 104.63 and 96.58 mm, it is much close to 105.074 mm. The mean load of 56.512 N is obtained for the profile Pr00 without cutout and profiles with various aspect ratios is shown in Figure 11 b), the increase in aspect ratio results in reduction of average mean load which varies from 9.2% to 19.83%. The above results indicates the variation in final deformation, collapse mode and peak force is influenced greatly by the aspect ratios of the cutouts. It also reveals that increase in major axis results in maximum deformation which in turn reduction in energy absorbing capacity of thin-walled tubes.

4.3 The Impact of Symmetry of the Cutout

In this section, the effect of symmetry of cutouts had investigated as a deformation control method in view of restricting the failure caused by the global collapse bending mode. The transfer of mode results in maximum energy absorption in thin-walled tubes. As revealed in section 4.1, if the cutout

is positioned at the mid-section of the tube which experiences higher stress concentrations around the cutout zone and its immediate outcome is transition of collapse mode to global bending. To perceive the importance of symmetry of cut-out and its impact on collapse mode, collapse starting point, crash force efficiency (CFE) and specific energy absorption (SEA) are investigated. In order to mitigate the effectiveness of the symmetry of geometrical discontinuities, three types of cutouts were selected and its interactions are depicted in Table 4, 5 and in Figure 12.
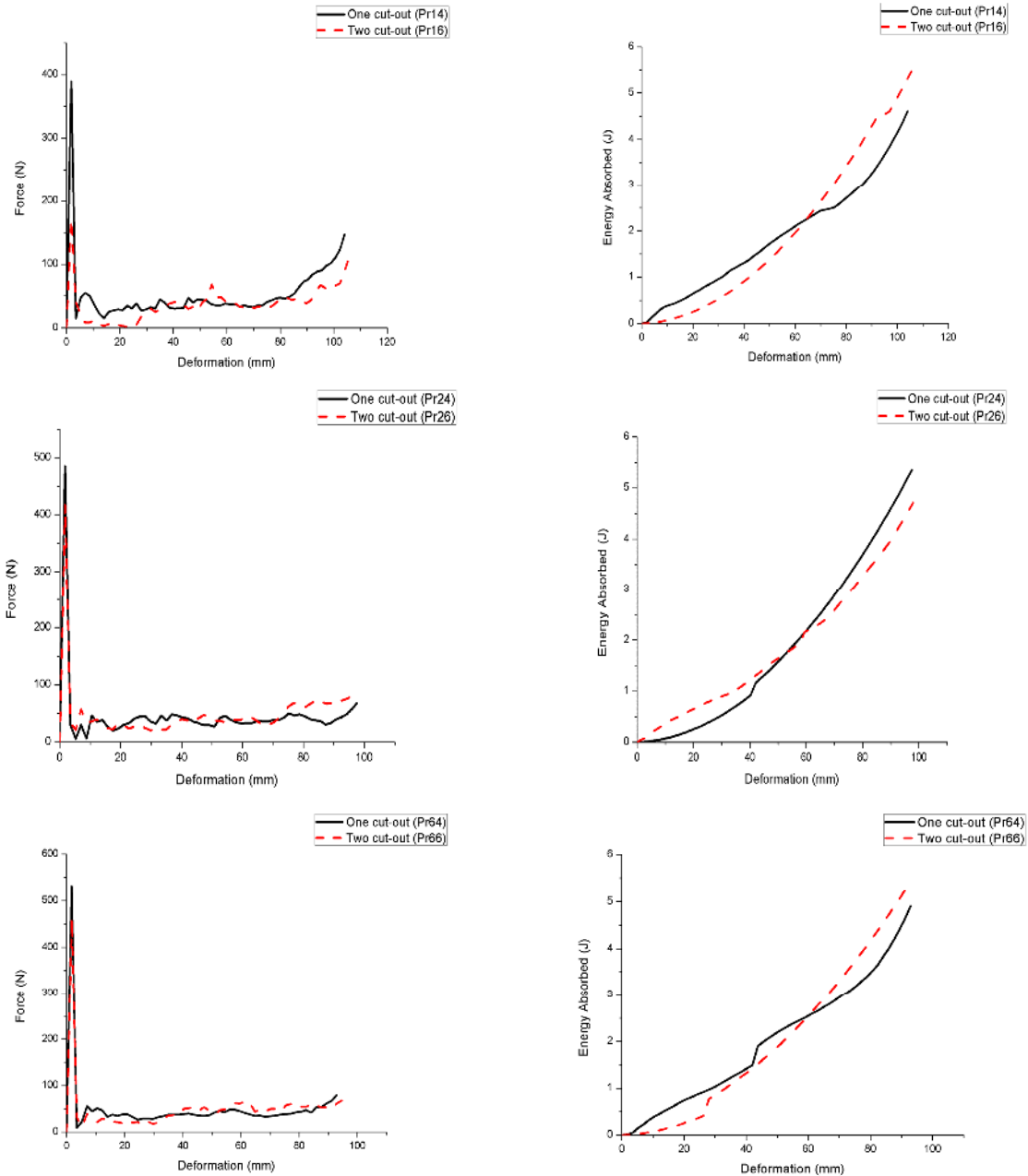

Figure 12: Interaction between forcé-deformation history and energy
absorption- deformation curves subject to quasi-static loading.

Furthermore, the introduction of symmetry in cut-out results in transition of collapse mode from global bending to progressive folding. Similarly, for the specimen Pr14 and Pr16 with major axis length of 24.5 mm is compared. The results from these cases exhibits variation of collapse mode pattern from concertina and diamond to completely diamond mode. Furthermore, the variation in collapse pattern makes the significant decrease in peak load and energy absorption. It can be noticed that the variation in maximum peak force of 389.25N to 169.81N for the specimen for Pr14 and Pr16 respectively. The observed variation is due to the symmetry of the cutout, it can be noticed that the specimen having symmetrical cutout will be much effective than the one having the single cutout when it is subjected to same testing conditions.

Moreover, increase in major axis of cutout provokes in depth fact of increase in energy absorption rate of 4.608 J to 5.504 J, it indirectly increases the crash force efficiency(CFE) from 13.50 to 14% and its impact on specific energy absorption (SEA) from 1950.88 to 2330.222 (J/kg) for the observed specimen Pr14 and Pr16 is clearly visible. Figure 12 shows the interaction between force and deformation along with deformation and energy absorption of various specimens having one and two cutouts.

4.4 Deformation (or) Collapse Mode

The deformed sections of experimental and analytical samples are scrutinized in Figure 9. It is evident that there are considerable differences between the above in some cases, due to the non-uniformities in forming cut-outs in the fabrication process. The obtained collapse modes for each case are given in Table 5. Furthermore, the increase in major axis of cutout shows the transition of collapse mode from completely diamond to concertina and diamond mode. Also the collapse starting point is change from mid of specimen to the moving end. The triangular formation experienced by the specimen, at the start of the quasi-static process shown in Figure 13.
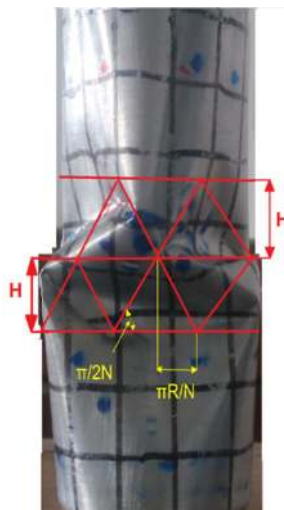
Figure 13: Formation of triangular lobes at the start of quasi-static process.

4.5 Energy Absorption

The energy absorption capability of tested thin walled tubes with various locations of Lo is clearly depicted in Table 4 and Figure 14. It is clear from these figures increase in Lo, i.e. nearer to the loading end increases the energy absorption rate irrespective to the aspect ratios. For instance, specimen Pr11 whose cutout location is 0.375L experiences energy absorption rate of 3.226 J. Similarly for specimen Pr15 whose major axis length is 24.5 mm similar to the profile Pr11, only change made is the cutout location transferred to 0.875L experiences 4.877 J. The percentage increase in energy absorption rate is about 33.05%, is mainly due to the transition of collapse modes from irregular progressive folding to global bending mode. The origin of collapse starting point is gradually shifted over from mid of the specimen to the moving end of the impactor. The observed result is unanimously similar to the entire specimen irrespective to their aspect ratios, if the location of the cutout is nearer to the impactor it results in higher energy absorption rate for the corresponding aspect ratios.

4.6 Maximum Collapse and Mean Load

The maximum force (P_{max}) is the demanding parameter during quasi-static (or) impact loading and the first peak observed in force-deformation curve. Investigations of these parameter displays for all aspect ratios, occurrence of collapse mode is of diamond and origin of collapse point is normally mid-of the specimen. However, the maximum force could be reduced by introducing the triggering dents or other folding initiators. It is evident that the same effect can be obtained by introducing of symmetry of the cutouts what we had briefed in Pr16, Pr26 and Pr66. For instance Pr14 exhibits the maximum peak force of 389.25 N, by introducing symmetry for the specimen Pr16 it is drastically reduced to 169.81N of percentage reduction about 56.37% is very encouraging. The increase in aspect ratio results in reduction of mean load, in concern with energy absorbing systems the need for decrease in the difference between maximum and average forces is essential. It is normally done by filling foams, providing external grooves on the peripheral of the tubes or using variable thickness tubes (VTD).

$$P_{mean} = \frac{\sigma_y t^2}{2\sqrt{3}} \left(\frac{4\pi H}{t} - \frac{\pi N}{3} \right) \cdot \left(1 + \frac{V_0}{2DC} \right)^{1/p} \tag{13}$$

Also, experimental and numerical studies have proved that thin-walled tubes with higher D/t ratio (i.e., 5098) and strain hardening makes material sensitive which leads to occurrence of collapse pattern in the form of diamond mode. It could be observed that the stability of the crushing process and the corresponding energy absorption was much higher for the specimens possessing shorter major axis length. The load bearing capacity is greatly influenced by the type of cut-out. The longer major axis forms the short and flat hole which is perpendicular to the direction of compression load. The resistance experienced to the external forces is not efficient; it directly affects the load bearing capacity and further causes the different collapse modes results in significant reduction in mean load (P_{mean}) for the occurred deformation. By location (i.e., Lo= 0.75L), the specimen experiences significant reduction in crushing force due to the formation of plastic hinges which results in similar maximum force (P_{max}). The similar maximum force (P_{max}) and reduction in mean load (P_{mean}) directly affects the overall crash force efficiency. The specimen Pr 44 experiences the comparatively least CFE in the process. In Figure 15, the comparison between the numerical and experimental results

are exhibited which has more similarities. The validation of the obtained results for the mean load of the specimen (Pr14) obtained in experimental mode is compared with the analytical from (Palanivelu et al., 2011). The obtained (P_{mean}) value by using the equation (13) is 50.5 N, similarly the obtained analytical result is compared with the experimental data and numerical simulation which is of 52.57 N and 54.786N. The difference in percentage is about 3.93 %, which gives the confidence in continuing the research.
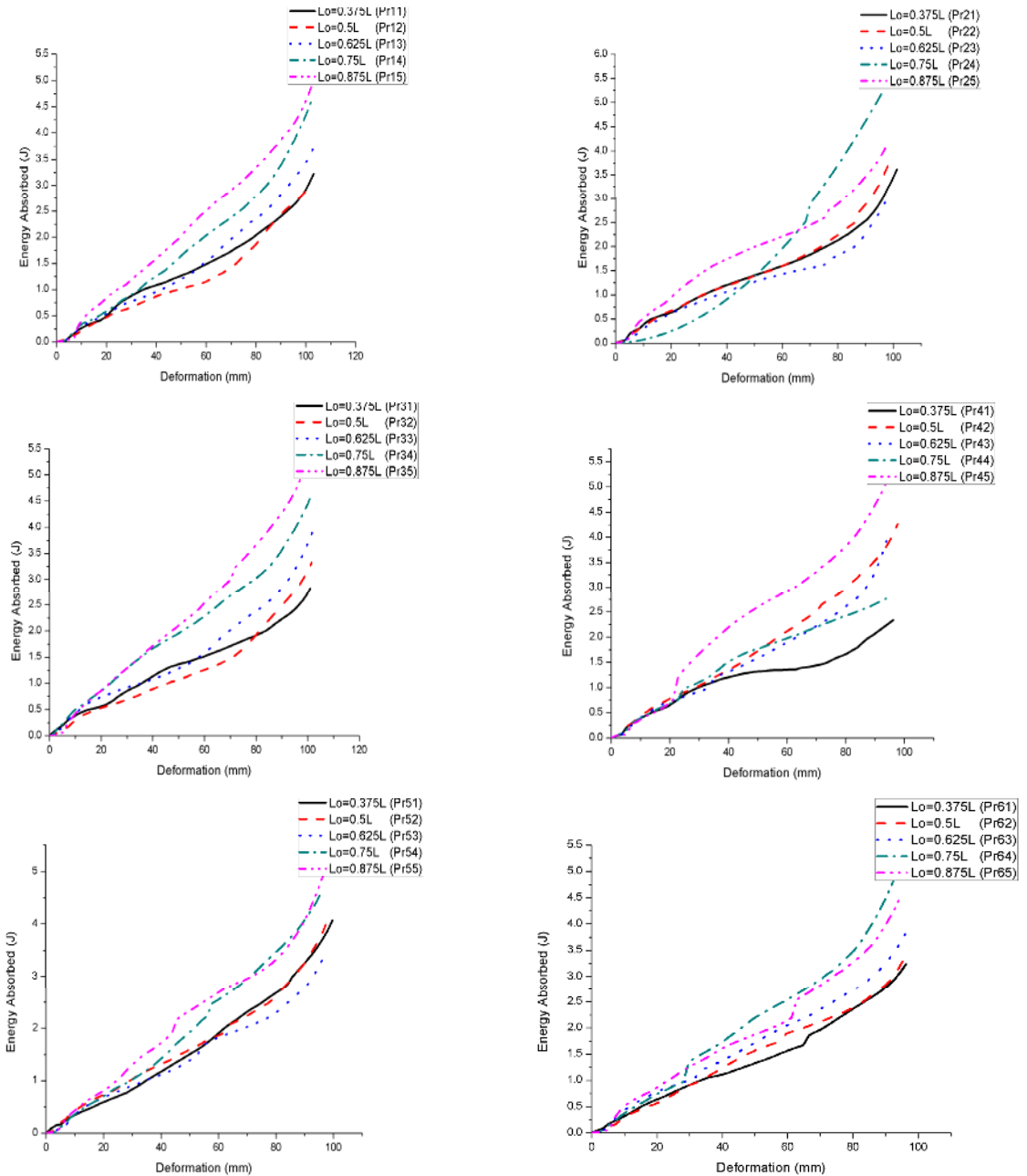

Figure 14: Interaction between forcé-deformation history and deformation-energy absorption curves subject to quasi-static loading.
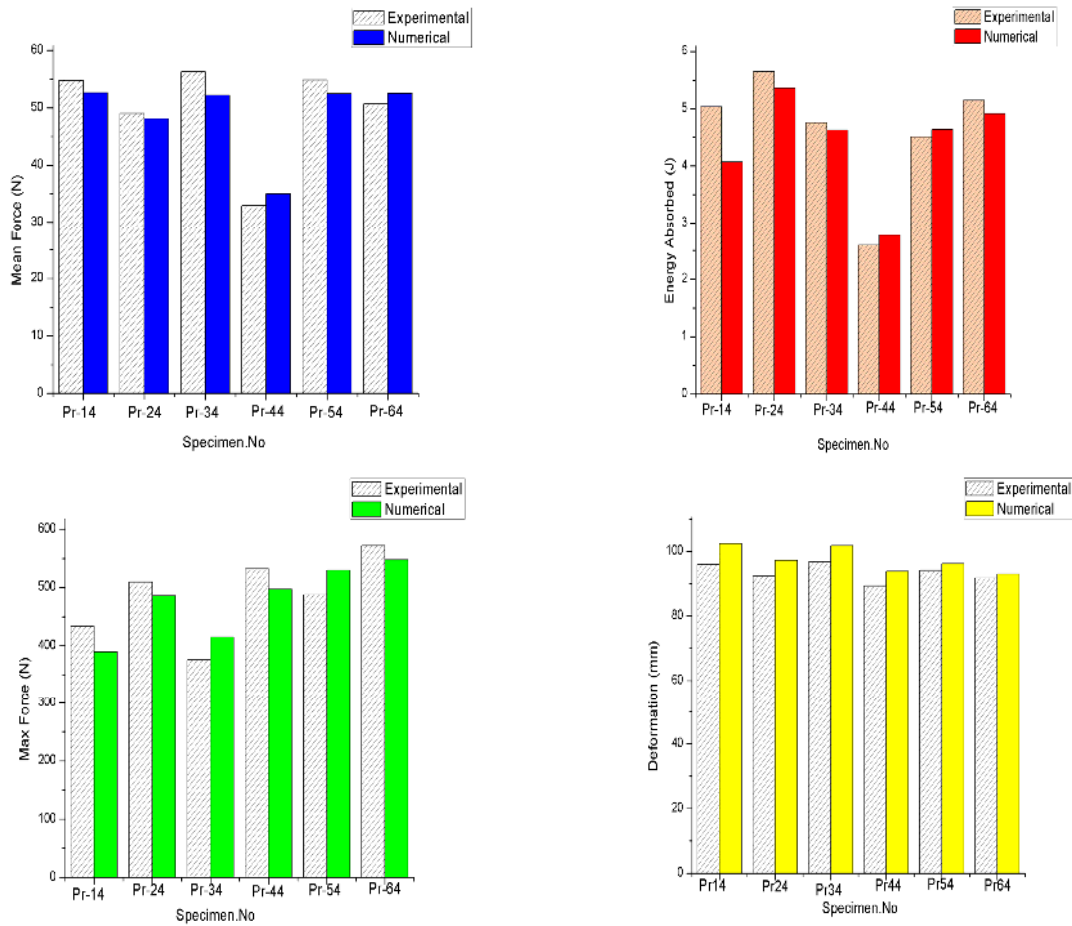
Figure 15: Interaction between forcé-deformation history and deformation-energy
absorption curves subject to quasi-static loading.

5 CONCLUSIONS

The significant outcome related to the thin-walled tubes from experimental and numerical observation which may be used as energy absorbers are given below:

- The location of cut-out can drastically influences the energy absorption and buckling characteristics of the thin-walled tubes.
- The presence of cut-out with higher major axis length reduces the maximum peak force, causes the greater crushing deformation of thin-walled structures.
- The mean buckling values (P_{mean}) decreases linearly as the function of elliptical discontinuities with the increase in cut-out major axis length.
- By increasing the cut-out location from mid-height of the tube towards moving end, shows reduction in peak buckling force (P_{max}) and considerable increase in energy absorption capability irrespective of aspect ratios.
- It is worth noting that a transition of collapse modes from concertina to diamond modes to completely diamond mode, when the two cut-outs were positioned at opposite faces.

- Absorbed energy per unit mass is larger for the profile with symmetric cut-outs, Specimen Pr16, Pr26, P66 obtained increase in energy absorption rate by 16.27%, 28.75%, 09.23% when compared to Pr14, Pr24, P64.
- The highest crash force efficiency (CFE) of 14% for the specimen Pr16 with elliptic symmetry cut-out, which contains the larger major axis length of 24.5 mm with the aspect ratio of 4.08.
- There is a good agreement between experimental data and simulation results, the analytical solution including the strain rate and strain hardening effects of the material gives the mean loads which are very close to experimental results.

Furthermore, if the thin-walled structures are designed with cutouts to obtain the expected results, the discontinuities with symmetry is a significant variable to consider.

References

Abramowicz, W., Jones, N., (1984). Dynamic axial crushing of circular tubes. International Journal of Impact Engineering 3: 263–281.

Abramowicz, W., Jones, N., (1984). Dynamic axial crushing of square tubes. International Journal of Impact Engineering 2: 179–208.

Ahmad, Z., Thambiratnam, D.P., (2009). Dynamic computer simulation and energy absorption of foam filled conical tubes under axial impact loading. International Journal of Computers and Structures 87: 186-197.

Alexander, J.M., (1960). An appropriate analysis of the collapse of thin cylindrical shells under axial loading. Quarterly Journal of Mechanics and Applied Mathematics 13: 10-15.

Chukwuemeke, W.I., and Oluleke, O., (2016). Energy absorption improvement of circular tubes with externally press fitted ring around tube surface subjected to axial and oblique impact loading. International Journal of Thin walled Structures 109: 352-366.

Chung, S.K.Y., Nurick, G.N., Starke R.A., (2008). The energy absorption characteristics of double cell tubular profiles, Latin American Journal of Solids and Structures 5: 289-317.

Darvizeh, A., Meshkinzr, A., Alitavoli, M., & Rajabiehfard, R., (2017). Low velocity impact of empty and foam filled circumferentially grooved thick-walled circular tubes. International Journal of Thin walled Structures 110: 97-105.

Dorin, D., Kaarstad, B.L., Skajaa, B., Hopperstad, O.S., Langseth, M., (2017). Testing and modeling of stiffened aluminium panels subjected to quasi-static and low-velocity impact loading. International Journal of Impact Engineering 00: 1-15. (in press)

Estrada, Q., Szwedowicz, D., Baltazar, M., Cortes, C., Majewski, T., & Estrada, C.A., (2016). The performance of energy absorption in structural profiles with different discontinuities. International Journal of Advanced Manufacturing Technology 84: 1081-1094.

Estrada, Q., Szwedowicz, D., Majewski, T., Oliver, M., Cortes, C., Estrada, C.A., Castro, F., (2016). Effect of discontinuity size on the energy absorption of structural steel beam profiles. International Journal of Advanced Materials and Structures 24: 88-94.

Fan, Z., Lu. G., Liu. K., (2013). Quasistatic axial compression of thin walled tubes with different cross sectional shapes. International Journal of Engineering Structures 55: 80-89.

Hou, S.J., Li, Q., Long, S.Y., Yang, S.J., (2007). Design Optimization of regular hexagonal thin walled columns with crashworthiness criteria. International Journal of Finite Element Analysis and Design 43: 555-565.

Huang, M.Y., Tai, Y.S., Hu, H.T., (2010). Dynamic characteristics of high strength steel cylinders with elliptical geometric discontinuities. International Journal of Theoretical and Applied Fracture Mechanics 54: 44-53.

Jones, N. (2011). Structural Impact, Cambridge University Press.

Kashani, M.H., Alavijeh, H.S., Akbarshahi, H., Shakeri, M., (2013). Bitubular square tubes with different arrangements under quasistatic axial compression loading. International Journal of Materials and Design 51: 1095-1103.

Khalkhali, A., Mostafapour, M., Tabatabaie, S.M., Ansari, B., (2016). Multi-objective crashworthiness optimization of perforated square tubes using modified NSGAII and MOPSO. International Journal of Structural Multidisciplinary Optimization 54: 45-61.

Nia, A.A., and Hamedani, J.H., (2010). Comparative analysis of energy absorption and deformations of thin walled tubes with various section geometries. International Journal of Thin walled Structures 48: 946-954.

Nia, A.A., Fallah Nejad, K.H., Badnava, H., Farhoudi, H.R., (2012). Effect of buckling initiators on mechanical behavior of thin-walled square tubes subjected to oblique loading. International Journal of Thin walled Structures 59: 87-96.

Niknejada, A., Abedia, M.M., Liaghab, G.H., & Zamani Nejad, M., (2012). Prediction of mean folding force during the axial compression in foam filled grooved tubes by theoretical analysis. International Journal of Materials and Design 37: 144-151.

Palanivelu, S., Van Paepegam, W., Degrieck, J., De Pauw, S., Vantomme, J., Wastiels, J., ... & Van Hemelrijck, D., (2011). Low velocity axial impact crushing performance of empty recyclable beverage cans. International Journal of Impact Engineering 38: 622-636.

Reid, S.R., Reddy, T.Y., Gray, M.D., (1986). Static and Dynamic axial crushing of foam-filled sheet metal tubes. International Journal of Mechanical Sciences 28: 295–322.

Szwedowicz, D., Estrada. Q., Cortes, C., Besdolla, J., Alvarez, G., Castro, F., (2014). Evaluation of energy absorption performance of steel square profiles with circular dis-continuities. Latin American Journal of Solids and Structures 11: 1744-1760.

Tai, Y.S., Huang, M.Y., Hu, H.T., (2010). Axial compression and energy absorption characteristics of high strength thin walled cylinders under impact load. International Journal of Theoretical and Applied Fracture Mechanics 53: 1-8.

Velmurugan, R., Muralikannan, (2009). Energy absorption characteristics of annealed steel tubes of various cross sections in static and dynamic loading. Latin American Journal of Solids and Structures 6: 385-412.

Weirzbicki, T., Abramowicz, W., (1983). On the crushing mechanics of thin walled structures. International Journal of Applied Mechanics 50: 727-734.

Zahran, M.S., Xue, P., Esa, S.Y., Abdalwaheb, M.M., Guoxing Lu., (2017). A new configuration of circular stepped tubes reinforced with external stiffeners to improve energy absorption characteristics under axial impact. Latin American Journal of Solids and Structures 14: 292-311.